

Cor Claeys
Eddy Simoen

SPRINGER SERIES IN MATERIALS SCIENCE 118

Fundamental and Technological Aspects of Extended Defects in Germanium

 Springer

Springer Series in
MATERIALS SCIENCE

Editors: R. Hull R. M. Osgood, Jr. J. Parisi H. Warlimont

The Springer Series in Materials Science covers the complete spectrum of materials physics, including fundamental principles, physical properties, materials theory and design. Recognizing the increasing importance of materials science in future device technologies, the book titles in this series reflect the state-of-the-art in understanding and controlling the structure and properties of all important classes of materials.

- | | | | |
|-----|---|-----|---|
| 99 | Self-Organized Morphology in Nanostructured Materials
Editors: K. Al-Shamery and J. Parisi | 109 | Reactive Sputter Deposition
Editors: D. Depla and S. Mahieu |
| 100 | Self Healing Materials
An Alternative Approach to 20 Centuries of Materials Science
Editor: S. van der Zwaag | 110 | The Physics of Organic Superconductors and Conductors
Editor: A. Lebed |
| 101 | New Organic Nanostructures for Next Generation Devices
Editors: K. Al-Shamery, H.-G. Rubahn, and H. Sitter | 111 | Molecular Catalysts for Energy Conversion
Editors: T. Okada and M. Kaneko |
| 102 | Photonic Crystal Fibers
Properties and Applications
By F. Poli, A. Cucinotta, and S. Selleri | 112 | Atomistic and Continuum Modeling of Nanocrystalline Materials
Deformation Mechanisms and Scale Transition
By M. Cherkaoui and L. Capolungo |
| 103 | Polarons in Advanced Materials
Editor: A.S. Alexandrov | 113 | Crystallography and the World of Symmetry
By S.K. Chatterjee |
| 104 | Transparent Conductive Zinc Oxide
Basics and Applications in Thin Film Solar Cells
Editors: K. Ellmer, A. Klein, and B. Rech | 114 | Piezoelectricity
Evolution and Future of a Technology
Editors: W. Heywang, K. Lubitz, and W. Wersing |
| 105 | Dilute III-V Nitride Semiconductors and Material Systems
Physics and Technology
Editor: A. Erol | 115 | Lithium Niobate
Defects, Photorefractive and Ferroelectric Switching
By T. Volk and M. Wöhlecke |
| 106 | Into The Nano Era
Moore's Law Beyond Planar Silicon CMOS
Editor: H.R. Huff | 116 | Einstein Relation in Compound Semiconductors and Their Nanostructures
By K.P. Ghatak, S. Bhattacharya, and D. De |
| 107 | Organic Semiconductors in Sensor Applications
Editors: D.A. Bernards, R.M. Ownes, and G.G. Malliaras | 117 | From Bulk to Nano
The Many Sides of Magnetism
By C.G. Stefanita |
| 108 | Evolution of Thin-Film Morphology
Modeling and Simulations
By M. Pelliccione and T.-M. Lu | 118 | Extended Defects in Germanium
Fundamental and Technological Aspects
By C. Claeys and E. Simoen |

Volumes 50–98 are listed at the end of the book.

Cor Claeys
Eddy Simoen

Extended Defects in Germanium

Fundamental and Technological Aspects

With 231 Figures

 Springer

Professor Dr. Cor Claeys

Dr. Eddy Simoen

Katholieke Universiteit Leuven, Interuniversity Microelectronics Center (IMEC)

Kapeldreef 75, Heverlee, 3001 Leuven, Belgium

E-mail: claeys@imec.be, simoen@imec.be

Series Editors:

Professor Robert Hull

University of Virginia

Dept. of Materials Science and Engineering

Thornton Hall

Charlottesville, VA 22903-2442, USA

Professor Jürgen Parisi

Universität Oldenburg, Fachbereich Physik

Abt. Energie- und Halbleiterforschung

Carl-von-Ossietzky-Strasse 9-11

26129 Oldenburg, Germany

Professor R. M. Osgood, Jr.

Microelectronics Science Laboratory

Department of Electrical Engineering

Columbia University

Seeley W. Mudd Building

New York, NY 10027, USA

Professor Hans Warlimont

Institut für Festkörper-

und Werkstofforschung,

Helmholtzstrasse 20

01069 Dresden, Germany

Springer Series in Materials Science ISSN 0933-033X

ISBN 978-3-540-85611-5

e-ISBN 978-3-540-85614-6

Library of Congress Control Number: 2008935633

© Springer-Verlag Berlin Heidelberg 2009

This work is subject to copyright. All rights are reserved, whether the whole or part of the material is concerned, specifically the rights of translation, reprinting, reuse of illustrations, recitation, broadcasting, reproduction on microfilm or in any other way, and storage in data banks. Duplication of this publication or parts thereof is permitted only under the provisions of the German Copyright Law of September 9, 1965, in its current version, and permission for use must always be obtained from Springer-Verlag. Violations are liable to prosecution under the German Copyright Law.

The use of general descriptive names, registered names, trademarks, etc. in this publication does not imply, even in the absence of a specific statement, that such names are exempt from the relevant protective laws and regulations and therefore free for general use.

Typesetting: Data prepared by SPi using a Springer \TeX macro package

Cover concept: eStudio Calamar Steinen

Cover production: WMX Design GmbH, Heidelberg

SPIN: 12222698 57/3180/SPi

Printed on acid-free paper

9 8 7 6 5 4 3 2 1

springer.com

Preface

Extended defects in semiconductors are usually considered detrimental. In the early days of electronic devices, only polycrystalline material was available. In fact, germanium was the first material that could be grown dislocation free, the reason being its relatively low melting point. With the improvement of crystal growth, dislocation-free wafers became available and are nowadays the standard in the case of 200 and 300 mm diameter silicon substrates. In the future, there may even be a switch over to a 450 mm wafer size. In the case of Ge it is already feasible to grow 300 mm dislocation-free wafers. On the other hand, low-cost, solar-grade silicon material is characterized by the presence of a large density of extended defects: grain boundaries, twins, dislocations and stacking faults, which determine to a large extent its electrical performance and solar energy conversion efficiency. Other applications, like detectors for nuclear radiation spectroscopy, require a density of dislocations in the range of a few hundreds to thousands for a successful, high-resolution operation. It implies that depending on the application, extended defects may be present and, therefore, their electrical and mechanical effects should be studied and well-characterized. Giving the current interest in renewable energy, and in particular, solar energy, it comes as no surprise that the study of extended defects in semiconductors is experiencing a second youth, with a great deal of research activities going on world-wide, involving a growing number of young scientists.

At the moment, the main application of Ge wafers is space solar cells, requiring high-quality defect-free material. Ge can be a potential block-buster, as channel material for sub-22 nm CMOS. However, transistors will be made only on thin Ge layers fabricated on a silicon handle or carrier wafer. Whatever the fabrication technique of choice, i.e., epitaxial deposition, Ge condensation or smart-cut GeOI, extended defects may readily be formed, so that the understanding of the formation and the control of extended defects is of crucial importance in state-of-the-art Ge materials. The main reason for the formation of misfit and threading dislocations is the lattice mismatch between the substrate - usually silicon - and the epitaxial layer, which amounts to about

4.1% at room temperature for pure Ge. It implies that below a certain critical thickness, which is about 1 nm for Ge, the layer can be deposited pseudomorphically, i.e., defect free, while above this thickness, plastic relaxation at the epitaxial interface readily occurs. Depending on the growth conditions, misfit dislocations are formed with threading arms reaching through the layer to the surface. It is in the first instance that these threadings can be harmful for device operation and should be controlled to acceptable levels, either during growth or by a post-deposition annealing treatment.

On the other hand, extended defects may be created also during device processing, as it is known that certain steps like ion implantation, dry etching or device isolation create damage and/or stress which eventually, upon annealing, develop into extended defects. Also thermal stresses during processing may relax into dislocations or related extended defects. Whatever the application or device structure, p-n junctions are generally an inherent part of it and the fabrication method of choice in industry is by ion implantation, as it allows a precise control of the junction depth and sheet resistance. The penalty paid is the formation of point and extended defects, which are the result of the clustering of the displaced lattice atoms and the associated vacancies. This clustering occurs during the post-implantation annealing, necessary to activate the dopants.

In view of these issues, defect engineering has become a mature and exciting field of expertise in the silicon world but lacks thousands of man-years of research in the case of Ge processing. The understanding of processes like ion implantation-damage annealing or solid-phase epitaxial regrowth, point-defect engineering for dopant diffusion control, etc. are far less well-developed in the case of Ge and, therefore, require renewed interest. The concept of gettering, where beneficial use is made of extended defects to remove detrimental metallic contaminants from the active device regions, and playing a crucial role in yield engineering in the IC industry, hardly exists for germanium. It is the aim of this book to fill this gap and form a bridge between the fundamental material studies carried out mainly in the fifties and sixties and today's practice and research interests. Defect formation in state-of-the-art processing modules intended for sub 32 nm technology nodes will be used to illustrate the theoretical and physical defect studies.

The aim is to give an overview of the physics of extended defects in germanium, i.e., dislocations (line defects), grain boundaries, stacking faults, twins and $\{311\}$ defects (two-dimensional defects) and precipitates, bubbles, etc. The first chapter will be more fundamental, describing the crystallographic structure and mechanical properties of dislocations, which have been established in the fifties and sixties, based on defect etching and optical or electron microscopy. Currently, focus is on *in situ* studies of dislocation properties in a transmission electron microscope. It will be pointed out that dislocations are essential for the plastic deformation of germanium. Methods will be described to analyse and image dislocations and to evaluate their structure. Another field of interest is the measurement of strain distribution with nanometer

scale resolution. Indentation studies at room temperature are useful for the understanding of high pressure phase transformations in Ge and for revealing the hardness properties of Ge and related alloys. Dislocations can also impact on the diffusion of impurities, as will be outlined in the last paragraph.

The second chapter deals with the electrical and optical properties of dislocations, which are crucial for device operation. An overview of the different models, describing the electron states, will be given, starting from the dangling bond model of Shockley and Read. While over the years, large progress has been made, a full understanding is still lacking due to the complexity of the problem. Besides the presence of dangling bonds in the core of the dislocation, which may reconstruct, the states associated with the strain field may split from the band edges. Moreover, impurities tend to aggregate in the strain field of a dislocation, giving rise to greater recombination activity. The combination of optical and electrical spectroscopy has led to the concept where the dislocation states form one-dimensional bands in the band gap of germanium (or silicon) instead of a single level, which depends on the line charge captured in it. Chapter 3 describes the mechanical and electrical properties of grain boundaries in Ge.

Chapters 4 and 5 deal more with today's problems, namely, with the formation of extended defects during the preparation of modern Ge substrates, including epitaxial deposition on Si, condensation of SiGe-on-Insulator and smart-cut or bonded material and the issue of extended defect formation during modern processing, for example, by ion implantation or laser annealing.

In brief, the book should provide a fundamental understanding of the extended-defect formation during Ge materials and device processing, providing ways to distinguish harmful from less detrimental defects and point out ways for defect engineering and control.

Key features:

- Intended for a wide audience including students, scientists and process engineers employed in material manufacturing, semiconductor research centres and universities
- State-of-the-art information available for the first time as an all-in-source
- Extensive reference list making it an indispensable reference book
- Complementary to the first book on Ge Materials and Devices, edited in 2007 by the same authors.

Finally, we acknowledge M. Caymax, P. Clauws, M.-L. David, G. Eneman, R. Loo, M. Meuris, A. Satta and L. Souriau for useful discussions and the use of some results. We also thank the IMEC Ge and III-V team.

Belgium
September 2008

Prof. Dr. Cor Claeys
Dr. Eddy Simoen

Contents

1	Dislocations in Germanium: Mechanical Properties	1
1.1	Introduction	1
1.2	Elastic Properties of Germanium	2
1.2.1	Definitions	2
1.2.2	Linear Expansion Coefficient of Ge	4
1.2.3	The First-Order Elastic Constants	6
1.2.4	Third-Order Elastic Constants	7
1.2.5	Internal Friction of Ge	8
1.3	Dislocation: Definitions and Structures	11
1.4	Creation and Observation of Dislocations	15
1.4.1	Grown-In Dislocations	17
1.4.2	Deformation-Induced Dislocations	18
1.4.3	Observation of Dislocations	19
1.5	Hardness and Plasticity of Ge at Room Temperature	24
1.6	High Temperature Plasticity of Germanium	30
1.6.1	Dislocation Velocity: Experimental Facts	31
1.6.2	Dislocation Velocity: Fundamental Understanding	41
1.6.3	Static Flow Tests or Creep Curve	42
1.6.4	Dynamic Testing: Stress–Strain Yield Curves in Ge	46
1.7	Impact of Dislocations on Dopant Diffusion	54
1.8	Conclusions	57
	References	58
2	Electrical and Optical Properties	65
2.1	Introduction	65
2.2	Electronic States of Dislocations	67
2.2.1	Read’s Acceptor Level Model	67
2.2.2	Schröter’s 1D Band Model	70
2.2.3	First Principles Calculations and EPR Results: Do DBs Exist in Split Dislocations?	75
2.2.4	One Dimensional Conduction Along Dislocations	77

2.2.5	Deformation-Induced Point Defects	83
2.2.6	Electrical Activity of Grown-In Dislocations	85
2.3	Impact of Dislocations on Carrier Mobility	89
2.4	Impact of Dislocations on Lifetime, Trapping, and Noise	93
2.4.1	Impact on Carrier Recombination	93
2.4.2	Impact on Low Frequency Noise	99
2.5	Impact of Dislocations on Ge Junction Devices	100
2.6	Impact of Dislocations on Optical Properties	104
2.6.1	Absorption and Recombination	107
2.6.2	Optical Recombination	110
2.6.3	Photoconductivity	113
2.6.4	Photoluminescence	126
2.7	Conclusions	131
	References	132
3	Grain Boundaries in Germanium	137
3.1	Introduction	137
3.2	Structure and Observation of Grain Boundaries	137
3.3	Electrical Properties of Grain Boundaries	141
3.4	Optical Properties of Grain Boundaries	150
3.5	Conclusions	151
	References	151
4	Germanium-Based Substrate Defects	153
4.1	Introduction	153
4.2	Epitaxial Deposition: Definitions	154
4.2.1	Modern Epitaxial Techniques	154
4.2.2	Epitaxial Growth Modes	158
4.3	Heteroepitaxial Strained Layers	159
4.3.1	Equilibrium Critical Thickness	160
4.3.2	Metastable Critical Thickness	163
4.3.3	Misfit and Threading Dislocation Densities	165
4.3.4	Strained Layer Dislocation Nucleation Mechanism	166
4.3.5	Dislocation Glide and Climb in Strained Layers	169
4.3.6	Dislocation Interaction Mechanisms	172
4.3.7	Elastic Relaxation by Surface Roughening	175
4.3.8	Strain Relaxation in Local Epitaxial Growth	178
4.4	Homoepitaxy of Germanium	180
4.4.1	Growth Modes	180
4.4.2	Growth Roughness and Epitaxial Breakdown at Low Temperatures	184
4.5	Heteroepitaxial Growth of Ge on Si	193
4.5.1	Initial Growth Mechanisms	195
4.5.2	Direct Layer-By-Layer Growth of Ge on Si	198
4.5.3	Growth of Thick Relaxed Ge Layers Directly on Si	203

4.5.4	Growth of Thick Relaxed Ge Layers by Means of a Graded Virtual Substrate.....	206
4.5.5	Selective Epitaxial Growth of Relaxed Ge on Si	210
4.5.6	Growth of Strained Ge and Si Layers and Si/Ge Superlattices	215
4.6	Defects in Germanium-On-Insulator Substrates	216
4.7	Summary and Conclusions	227
	References	228
5	Process-Induced Defects in Germanium	241
5.1	Introduction	241
5.2	Fundamental Ion Implantation Damage Mechanisms	242
5.3	Heavy Ion Induced Void Formation	254
5.4	Damage Annealing and Solid Phase Epitaxial Regrowth	257
5.5	Implantation Damage and Removal by Standard Dopant Ions ..	265
5.5.1	Lattice Site and Damage of Implanted Species in Ge ...	265
5.5.2	Boron Implantation in Ge	268
5.5.3	Al Implantation in Ge	277
5.5.4	P and As Implantation in Ge	278
5.5.5	{311} Interstitial Clusters in Ge	282
5.6	Oxygen Implantation in Ge and Ion Beam Mixing	283
5.7	Hydrogen-Related Extended Defects in Germanium	285
5.8	Conclusions	287
	References	288
	Index	293

List of Acronyms

AFM	Atomic force microscope
bcc	Body-centered cubic
BIC	Boron-interstitial complex
BPSG	Borophosphorosilicate glass
CA	Cyclic annealing
CC	Collision cascade
CDED	Critical damage energy density
CMOS	Complementary metal oxide semiconductor
CMP	Chemical mechanical polishing
CVD	Chemical vapor deposition
Cz	Czochralski pulling technique
DB	Dangling bond
DC	Direct current
DE	Dislocation exciton
DLTS	Deep level transient spectroscopy
EBIC	Electron beam induced current
ELO	Epitaxial lateral overgrowth
EOR	End of range
EPD	Etch pit density
EPR	Electron paramagnetic resonance
ESR	Electron spin resonance
FA	Furnace anneal
fcc	Face-centered cubic
FE	Free exciton
FWHM	Full width half maximum
GB	Grain boundary
GeOI	Germanium on insulator
GR	Generation-recombination
HEDG	Hydrogen enhanced dislocation glide
HP	High purity
HVTEM	High-voltage transmission electron microscope

XIV List of Acronyms

IR	Infrared
LPE	Liquid phase epitaxy
LT-MBE	Low temperature molecular beam epitaxy
LTO	Low temperature oxide
MB	Matthew–Blakeslee
MBE	Molecular beam epitaxy
MD	Misfit dislocation
MDD	Misfit dislocation density
MEMS	Mechanical electrical microsystems
MHAM	Multiple hydrogen annealing for heteroepitaxy
MILC	Metal-induced lateral crystallization
ML	Mono layer
PC	Photoconductivity
PD	Point defect
PL	Photoluminescence
RBS	Rutherford backscattering
REDM	Recombination enhanced dislocation motion
RHEED	Reflection high energy electron diffraction
rms	Root mean square
RP-CVD	Reduced pressure chemical vapor deposition
RT	Room temperature
RTA	Rapid thermal anneal
SCC	Space charge cylinder
SEG	Selective epitaxial growth
SEM	Scanning electron microscope
SF	Stacking fault
SGOI	SiGe on insulator
SK	Stranski–Krastanow growth mechanism for epitaxial layers
SL	Super lattice
SME	Surfactant mediated epitaxy
SOI	Silicon-on-Insulator
SPER	Solid phase epitaxial regrowth
SRH	Shockley–Read–Hall
STM	Scanning tunneling microscopy
TD	Threading dislocation
TDD	Threading dislocation density
TED	Transient enhanced diffusion
TEM	Transmission electron microscope
TRIM	Transport of ions in matter
UHV	Ultra high vacuum
UHV-TEM	Ultra high vacuum transmission electron microscope
VLS	Vapor–liquid–solid
VLSI	Very large scale integration
VS	Virtual substrate
VW	Volmer–Weber growth mechanism for epitaxial layers

List of Symbols

a_{ed}	Average spacing between acceptor states (cm)
a_0	Lattice parameter (cm)
a_f	Lattice parameter in the overlay film (cm)
a_P	Distance between neighbouring Peierls valleys (cm)
a_s	Lattice parameter of the substrate (cm)
b	Burger's vector modulus
B_T	Bulk modulus at constant temperature (dyne cm ⁻²)
c	Distance between dangling bonds (cm)
c_n	Recombination coefficient for electrons (cm)
c_p	Recombination coefficient for holes (cm)
C	Spacing between dangling bonds
C_f	Grading rate of a compositional film (% μm ⁻¹)
C_p	Specific heat at constant pressure
C_s	Solid solubility concentration (cm ⁻³)
C_V	Specific heat at constant volume
C_{xy}	Elastic parameters of the stress tensor (dyne cm ⁻²)
d	Bond length (m)
d_{GB}	Distance between grain boundaries (cm)
D	Diffusion length (cm)
D_a	Amorphization threshold dose (cm ⁻²)
E_A	Activation energy (eV)
E_B	Atomic bonding energy (eV)
E_C	Minimum of the conduction band (eV)
E_d	Energy level of the dislocation acceptor level (eV)
E_{dc}	Bond strain energy (eV)
E_d	Energy level of the dislocation acceptor level (eV)
E_{dis}^{eff}	Energy needed to displace a lattice atom (eV)
E_e	Electrostatic energy of the Coulombic interaction between the occupied DBs (eV)
E_F	Fermi level (eV)
E_G	Band gap energy (eV)

XVI List of Symbols

E_{gl}	Activation energy for dislocation glide (eV)
E_{FSK}	Formation energy for a single dislocation kink (eV)
E_i	Intrinsic activation energy of a dislocation (eV)
E_i	Interface energy (eV)
E_n	Dislocation nucleation barrier (eV)
E_0	Energy level of a neutral dislocation (eV)
E_{SK}	Activation energy for single kink motion (eV)
E_v	Activation energy for TD glide (eV)
E_V	Maximum of the valence band (eV)
f	Frequency (Hz)
f_{ed}	Fraction of the electrical active dangling bonds
f_m	Lattice mismatch
F	Electric field ($V\text{ cm}^{-1}$)
F_D	Damage fraction
g_s	Spin degeneracy factor
g_v	Valley degeneracy factor
G	Electron-hole generation rate ($\text{cm}^{-3}\text{s}^{-1}$)
G_s	Shear modulus (dyne cm^{-2})
G_0	Conductance at 0 V (mho)
G_{100}	Shear modulus in the $\langle 100 \rangle$ direction (dyne cm^{-2})
h	Planck's constant
h_c	Equilibrium critical thickness (cm)
h_e	Epilayer thickness (cm)
H	Hardness (kg/mm^2)
H_{KP}	Activation enthalpy of kink pair formation (eV)
H_V	Vickers hardness (kg mm^{-2})
I	Current (A)
I_r	Thermionic emission current per area (A cm^{-2})
I_s	Hole saturation current per area (A cm^{-2})
J	Displacement rate ($\text{cm}^{-1}\text{s}^{-1}$)
k	Boltzmann constant
K	Curvature of the neutral plane
K_s	Isothermal compressibility ($\text{cm}^2\text{ dyne}^{-1}$)
l_{av}	Misfit dislocation length projected into the (001) plane (cm)
l_d	Characteristic length of the conductive elements of a dislocation (cm)
L	Average free length of a dislocation (cm)
L_{2D}	Two-dimensional Debye screening length
m	Empirical factor related to the doping dependence of the dislocation damping
M	Dislocation density in the Frank Read source
m_0	Rest mass of an electron (g)
n	Electron concentration (cm^{-3})
n_a	Atomic density of displaced atoms per unit volume
n_i	Intrinsic carrier concentration (cm^{-3})

n_k	Number of kinks per unit volume (cm^{-3})
n_0	Free electron concentration (cm^{-3})
N_A	Acceptor concentration (cm^{-3})
N_C	Density of states in the conduction band (cm^{-3})
N_{CC}	Number of displaced atoms per ion
N_d	Dislocation density (cm^{-2})
N_D	Donor concentration (cm^{-3})
N_{ii}	Number of atoms within a spheroid defined by the longitudinal and transversal straggling of the statistical damage distribution
N_m	Density of mobile dislocations (cm^{-2})
N_n	Number of nucleation sites per event
N_p	Etch pit density (cm^{-2})
N_s	DB volume density (cm^{-3})
N_s	Density of lineage boundary dislocations per cm
N_{TD}	Threading dislocation density (cm^{-2})
N_{MDi}	Misfit dislocation density corresponding with full relaxation
N_V	Density of states in the valence band (cm^{-3})
p_i	Hole concentration (cm^{-3})
p_{MD}	Average spacing between misfit dislocations
P	Pressure (Pa)
P_e	Applied load (kg)
q	Elementary charge (C)
Q	Charge density (e cm^{-1})
Q_d	Activation energy for point defect diffusion (eV)
Q_i	Reverse of internal friction
Q_v	Activation energy for dislocation velocity (eV)
R	Radius of the charge cylinder around a dislocation (cm)
R_c	Capture radius of a dislocation (cm)
R_d	Deposition rate (cm s^{-1})
R_g	Ideal gas constant
R_{gr}	Grading rate or mismatch per unit thickness
S_d	Surface recombination velocity (cm s^{-1})
t	Time (s)
t_i	Incubation time for plastic deformation (s)
t_s	Substrate thickness (cm)
T	Temperature (K)
T_D	Debye temperature of Ge (K)
T_{def}	Deformation temperature (K)
T_m	Melt temperature (K)
T_R	Temperature of the crystallized ingot (K)
T_s	Substrate temperature (K)
U	Energy of the intra-atomic Coulomb interaction between excess charge and electrons in the neutral charge state of a dislocation
v_d	Dislocation velocity (cm s^{-1})
v_{th}	Thermal velocity (cm s^{-1})

XVIII List of Symbols

V	Volume (m^3)
V_{bi}	Built in potential of a p-n junction (V)
V_{DR}	Ratio of an individual cascade volume to the transport cascade volume
W	Vibration energy at maximal strain (eV)
W_{d}	Depletion width (cm)
Y	Yield stress
Y_{100}	Young modulus in the $\langle 100 \rangle$ direction (dyne cm^{-2})
Y_{111}	Young modulus in the $\langle 111 \rangle$ direction (dyne cm^{-2})
Z	Atomic number

List of Greek Symbols

α	Angle between the dislocation line and the Burgers vector
α_e	Linear expansion coefficient
α_{IR}	Infrared absorption coefficient (cm^{-1})
β_{GB}	Ratio of thermionic emission over hole saturation current
γ	Grüneisen parameter
γ^{GB}	Capture rate at a grain boundary
γ^{SF}	Stacking fault energy (erg cm^{-2})
Δ	Dissociation width of a split dislocation (cm)
ε	Strain
$\dot{\varepsilon}$	Strain rate
ε_0	Permittivity of vacuum (F cm^{-1})
ε_{Ge}	Dielectric constant of Ge
η_0	Linear charge density on a dislocation in equilibrium
θ	Misfit angle or angle of inclination
θ_t	Twist angle
ϕ	Angle between dislocation line and $\langle 110 \rangle$ direction
Φ_{B}	Potential barrier around a charged dislocation
λ	Wavelength (cm)
μ	Translational displacement
μ_{h}	Hole mobility ($\text{cm}^2 \text{V}^{-1} \text{s}^{-1}$)
μ_{P}	Poisson's ratio
ν	Volume density of dislocation segments
ν_e	Energy available for elastic atomic displacements
ρ	Density of recombination centers on a dislocation line (cm^{-1})
ρ_{\parallel}	Conductivity parallel to the grain boundary
ρ_{\perp}	Conductivity perpendicular to the grain boundary
ρ_{n}	Areal density of dislocation nucleation sites (cm^{-2})
σ_{d}	Capture cross section (cm^2)
σ_{DC}	DC conductance (Ωcm^{-1})
σ_{micro}	Microwave conductance (Ωcm^{-1})

XX List of Greek Symbols

τ	Applied stress (dyne cm ⁻²)
τ_a	Misfit stress driving threading dislocation motion (dyne cm ⁻²)
τ_b	Back-stress from neighboring dislocation (dyne cm ⁻²)
τ_c	Critical shear stress (dyne cm ⁻²)
τ_C	Capture time constant (s)
τ_d	Bulk carrier lifetime (s)
τ_e	Extrinsic lifetime (s)
τ_{exc}	Critical excess stress (dyne cm ⁻²)
τ_{fill}	Filling pulse duration (s)
τ_i	Intrinsic lifetime (s)
τ_l	Lower yield point in stress-strain curve (dyne cm ⁻²)
τ_0	Actual shear stress needed to keep the dislocation velocity constant (dyne cm ⁻²)
τ_s	Shear stress (dyne cm ⁻²)
τ_t	Self-stress due to the line tension of the misfit dislocation length (dyne cm ⁻²)
τ_u	Upper yield point in stress-strain curve (dyne cm ⁻²)
ω	Optical Raman frequency
ω_s	Atomic density (at cm ⁻³)

Dislocations in Germanium: Mechanical Properties

1.1 Introduction

Germanium, having a face-centered cubic (fcc) diamond lattice, is brittle at room temperature like other Group IV semiconductors. This means that when applying a load on the material, it breaks before it deforms plastically. Gallagher [1], soon followed by some other Groups [2,3], was the first to report that when a stress is applied at high temperatures (in his work above 500°C) Ge becomes ductile. In other words, it deforms permanently by glide of dislocations (plastic flow). It was soon discovered that the glide planes were (111), that is, the planes of highest packing density in the structure [1–4], while the slip direction turned out to be $\langle 110 \rangle$ [5], the direction of the Burgers vector with modulus b .

As will be seen later, the plastic deformation of Ge is determined by the dynamic properties of the dislocations. The fact that Group IV elements are characterized by covalent bonding of four nearest neighbors gives rise to some unique mechanical behavior [6]. It is expected that the intrinsic dislocation or Peierls energy, taking into account the periodic structure of the lattice, is rather high in fcc diamond. This is related to the bonding rearrangement required in the core structure when moving a dislocation from one equilibrium site to another [6–8]. This means that at room temperature a high surface hardness is observed upon indentation, while at the same time the material breaks before it deforms. Another typical behavior is the yielding found in the stress–strain curve under dynamic load, using a constant strain rate $\dot{\epsilon}$ [6]. However, before dealing with the plastic flow of germanium, first, the elastic properties will be summarized and, more specifically, the first- and higher-order elastic constants discussed. They are keys to the understanding of the linear expansion coefficient (α_e) with temperature, which in turn is important for describing thermal stresses that may occur when a temperature gradient is present in the material or when two films with different α_e are in contact with each other (epitaxial growth).

In Sect. 1.3, some definitions will be given, and the possible structures of dislocations in the diamond lattice are described. Next, dislocation formation mechanisms are reviewed, followed by some experimental techniques for the observation of dislocations. In Sect. 1.5, the hardness of Ge at room temperature is discussed in the context of plastic flow or high-pressure phase transformation. The plastic flow at higher temperatures is the subject of Sect. 1.6, where a key feature is the velocity and multiplication of dislocations under a shear stress τ_s . It is well-known that dislocations can attract impurity atoms and point defects due to the elastic strain field surrounding them. This can lead to preferential precipitation and also to an enhanced diffusion along dislocation cores, as outlined in detail in Sect. 1.7.

1.2 Elastic Properties of Germanium

This section describes the elastic properties of germanium in terms of the first- and third-order elastic constants. In first paragraph, some basic material properties are defined. Next, the temperature dependence of the linear thermal expansion coefficient of Ge is given and discussed based on the Grüneisen parameter. In the third paragraph, the temperature dependence of the three first-order elastic constants is given, followed by the behavior of the third-order constants. Finally, the internal friction behavior of germanium is reviewed from which relevant information regarding the elastic properties of the material can be derived. For an introduction to the elastic properties of crystalline solids, the review by Huntington [9], for example, may be consulted.

1.2.1 Definitions

The elasticity of a diamond cubic Group IV semiconductor material is described in terms of the first-order elastic constants. In this regime, the strain is linearly dependent on the stress, and the relationship is known as Hooke's law. The 36 term fourth-order modulus tensor of Si or Ge can, based on symmetry arguments, be reduced to three terms, which are symbolized by C_{11} , C_{12} , and C_{44} and are related to the Young's modulus in the direction $\langle 100 \rangle$ (Y_{100}), $\langle 111 \rangle$ (Y_{111}), and the shear modulus G_s in $\langle 100 \rangle$ (G_{100}) [10] as follows:

$$C_{11} = 1/Y_{100}, \quad (1.1a)$$

$$C_{44} = 1/G_{100}, \quad (1.1b)$$

$$C_{12} = 3/2Y_{111} - 1/2Y_{100} - 1/2G_{100}. \quad (1.1c)$$

These constants are intimately related to how (acoustic) vibrations are propagated and absorbed in the material. The Young's moduli are derived from the resonant frequencies in the longitudinal direction, while G_s is the torsion or shear modulus (deformation in the transverse direction of the applied force).

From an atomistic perspective, Y_{100} at 0 K can be expressed as being proportional to $E_B(0)/d^3(0)$ [11], with E_B the atomic bonding energy and d the bond length. The softening of Young's modulus with higher temperature T can be described by considering the temperature dependence of E_B and d , given by [11]

$$E_B(T) = E_B(0) - \int_0^T C_V(y) dy, \quad (1.2a)$$

$$d(T) = d(0) \left[1 + \int_0^T \alpha_e(y) dy \right], \quad (1.2b)$$

with $C_V(T)$ the specific heat or heat capacity at a constant volume and $\alpha_e(T)$ the temperature-dependent linear thermal expansion coefficient or thermal volume expansivity. For Ge, this parameter is found experimentally to be given by [12]

$$\begin{aligned} \alpha_e(T) = & 6.05 \times 10^{-6} + 34.22 \times 10^{-9} (T - 273) \\ & - 0.35 \times 10^{-12} (T - 273)^2. \end{aligned} \quad (1.3)$$

This leads to a first-order linear reduction of Y_{100} with T , described by [11]

$$Y_{100}(T) = Y_{100}(0) [1 - BT] \quad (1.4)$$

and represented in Fig. 1.1. It has been shown that the slope of the temperature dependence $B_{\text{exp}} \sim C_V/E_B(0)$, with $E_B(0) = 2.58$ eV for Ge [11] and $C_V = 3R_g$ for $T \geq T_D$, with R_g the ideal gas constant and T_D the Debye temperature, which is 360 K for Ge [11]. The leveling-off of Y_{100} at low temperatures stems from the smaller $\int_0^T C_V(y) dy$ values because of the T^3 approximation at low temperature [13–17]. It has been demonstrated that $Y_{100}(T)/Y_{100}(0) = [\omega(T)/\omega(0)]^2$, with ω the optical Raman frequency, establishing a direct link between the thermally driven softening of the elasticity and bond expansion and vibration in the Ge lattice [11].

From the three first-order elastic constants, one can derive the compressibility K_s and Poisson's ratio μ_P [9]. For small pressures (P) in cubic crystals, one finds for the isothermal compressibility or the inverse bulk modulus B_T^{-1}

$$B_T^{-1} = K_s = -[\partial V/\partial P]_T/V = 3(C_{11} + 2C_{12}), \quad (1.5)$$

with V the atomic volume. This parameter increases with increase in temperature. The Poisson's ratio μ_P is given by [9]

$$\mu_P = -C_{12}/C_{11} \quad (1.6)$$

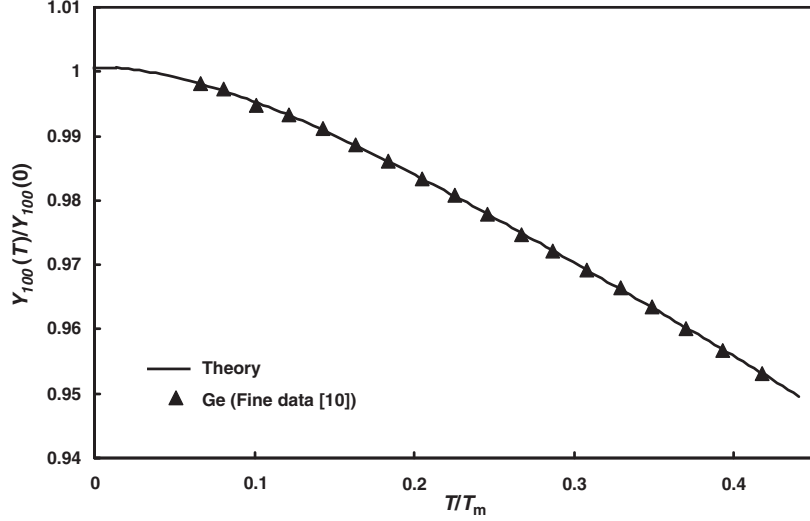


Fig. 1.1. Agreement between calculated and measured temperature dependence of Young's modulus for Ge, based on the model of (1.1)–(1.3). T_m is the melt temperature. The experimental data are from [10] (after [11])

and is nearly temperature-independent [10]. An important parameter related to the temperature dependence of the thermal expansion coefficient is the Grüneisen parameter γ [10, 18–19], used to describe the anharmonic properties of solids, defined by the relation [10]

$$\gamma = \alpha_e 3V / K_s C_P = \alpha_e 3V / K_t C_V, \quad (1.7)$$

with C_P the heat capacity at constant pressure. Normally γ is only weakly temperature-dependent in the low temperature range and in the case of Ge equal to 0.65 at -173°C and 0.74 at -73°C . The Grüneisen parameter is lower for both Si and for compound semiconductors such as GaAs, InAs, and InSb. In most cases there exists a correlation with the Debye temperature of the material. The atomic volume can be calculated based on the lattice parameter, which has been determined as $a_{20^\circ\text{C}} = 5.65748 \text{ \AA}$ at 20°C , while the density is $5.3234 \pm 0.00025 \text{ g cm}^{-3}$ at 25°C [11].

1.2.2 Linear Expansion Coefficient of Ge

The expansivity of Ge at low temperatures has been studied by several groups [18–26]. One of the striking features, obvious in Fig. 1.2, is the fact that α_e becomes negative for a reduced temperature $T/T_D = 0.04$. Below $T/T_D = 0.04$ again positive α_e is obtained, which can be described by a T^4 dependence [19]. This anomalous behavior of α_e for several diamond-like materials can be understood within the scope of the quasi-harmonic oscillator model in terms of

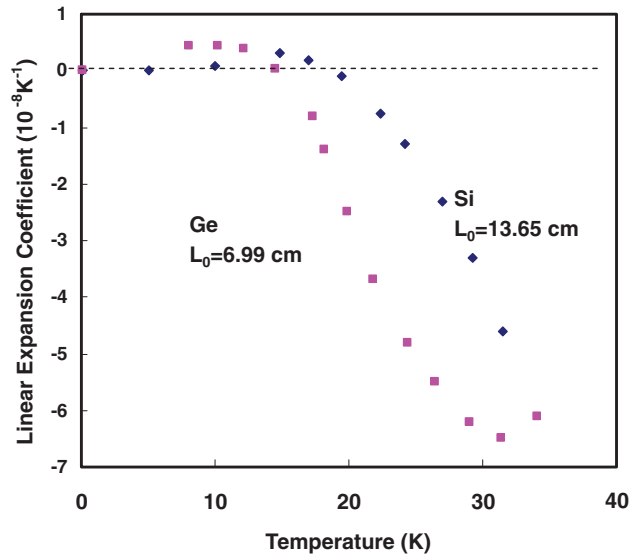


Fig. 1.2. Linear thermal expansion-coefficient data for Ge and Si (after [19])

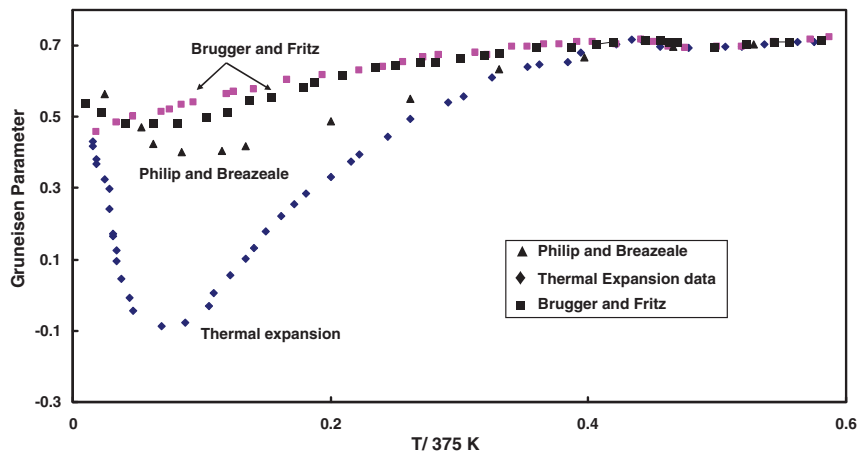


Fig. 1.3. Grüneisen parameter of germanium plotted as a function of the reduced temperature. The Brugger and Fritz method has been described in [18], and the thermal expansion data come from [19] (after [26])

the temperature dependence of the Grüneisen parameter [26–28]. The latter represents the strain derivative of the lattice vibration frequencies. Several experimental and theoretical estimates of γ have been performed in the past, which are summarized in Fig. 1.3 [26]. From this, it is clear that there is still insufficient theoretical understanding to explain the negative γ derived from

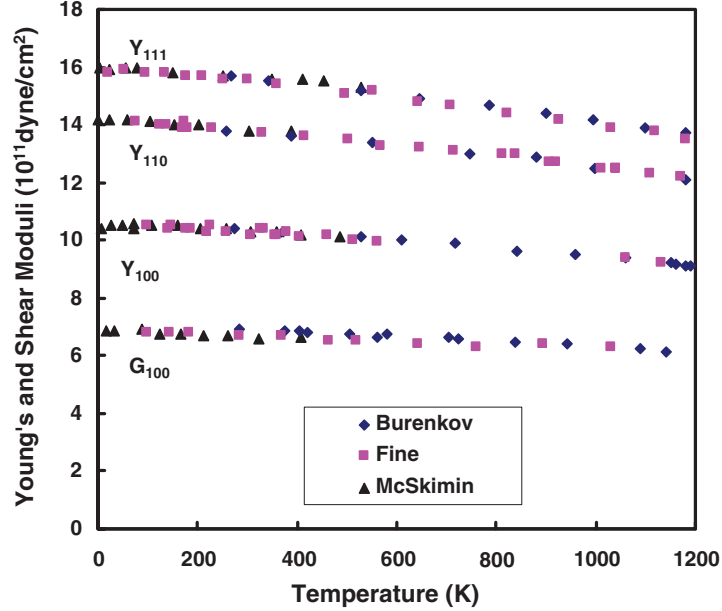


Fig. 1.4. Temperature dependences of Young's (Y_{111}), Y_{100} and Y_{110} and shear (G_{100}) moduli. Results reported by [10, 32, 33, 37] (after [37])

thermal expansion. It should be remarked that α_e is also slightly depending on the doping density, increasing with hole concentration in p-type Ge [29].

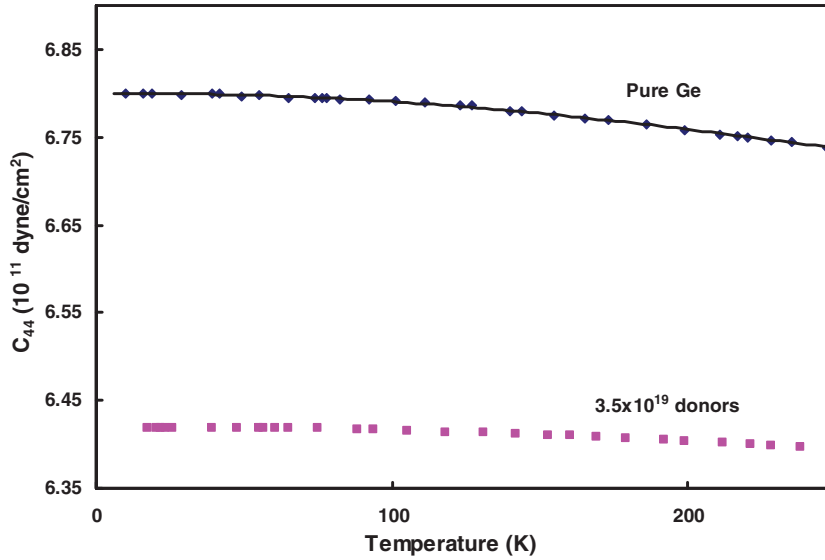
1.2.3 The First-Order Elastic Constants

The first-order elastic constants have been measured at both low [9, 30–35] and high temperatures [36–38]. It was found that they reduce in the first instance linearly with increasing temperature [36–38], as shown in Fig. 1.4 [37]. This is in agreement with the theory of anharmonicity of crystals. Values for C_{11} , C_{12} , and C_{44} at 25°C and for some other mechanical properties of Ge are summarized in Table 1.1 [39].

As theoretically predicted by Keyes [40], the elastic constants of Ge also depend on the doping concentration [41–43]. This is shown in Fig. 1.5 for the case of heavy n-type doping [41]. The reduction of C_{44} in Fig. 1.5 is related to the electronic contribution to the strain energy function. Since the elastic constants are the strain derivatives of the free energy of the crystal, it is assumed that heavy doping reduces the electronic contribution to the latter. Based on this hypothesis, a value for the shear deformation potential constant of 17.0 ± 0.2 eV was derived from experiments on heavy n-type material [42]. A similar value was obtained at liquid nitrogen temperature, while it was 19.2 eV at 4.2 K [42].

Table 1.1. Mechanical properties at 300 K of silicon and germanium

	Silicon	Germanium
[100] Young's modulus (10^{11} dyne cm^{-2})	13.0	10.3
[100] Poisson's ratio	0.28	0.26
Bulk modulus (10^{11} dyne cm^{-2})	9.8	7.13
Shear modulus (10^{11} dyne cm^{-2})	5.2	4.1
Hardness (Mohs)	7	6
Density (g cm^{-3})	2.329	5.323
C_{11} (10^{11} dyne cm^{-2})	16.60	12.60
C_{12} (10^{11} dyne cm^{-2})	6.40	4.40
C_{44} (10^{11} dyne cm^{-2})	7.96	6.77


Fig. 1.5. The temperature dependence of C_{44} in pure and heavily doped n-type germanium (after [41])

1.2.4 Third-Order Elastic Constants

Studies have also been performed of the third-order elastic constants [26, 42, 44–49]. These are related to the anharmonicity of the crystal, in other words, the nonlinearity of the interatomic forces with respect to atomic displacements. The third-order constants are important for some material properties like the thermal expansion, thermal conductivity, crystal stability, and fracture [46]. There are in total six independent third-order elastic constants in a cubic crystal called C_{166} , C_{112} , C_{111} , C_{456} , C_{144} , and C_{123} . Again, there

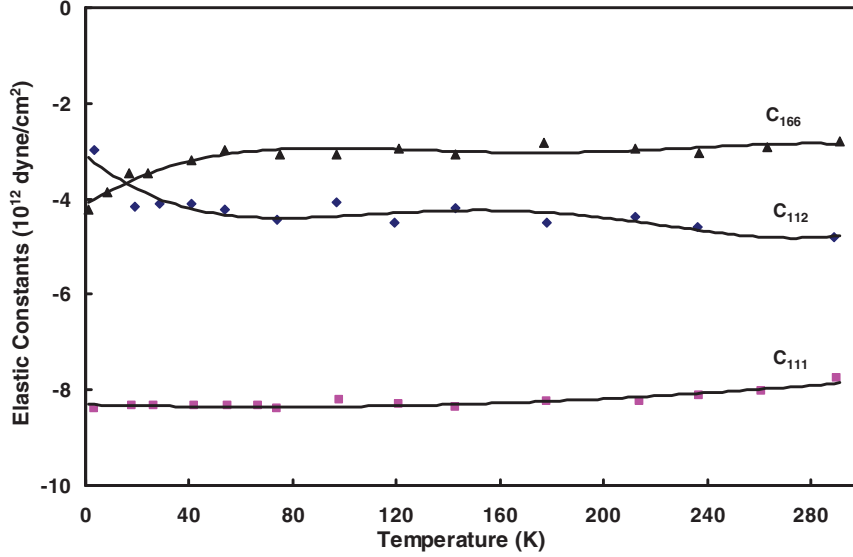


Fig. 1.6. Temperature variation of the third-order elastic constants C_{111} , C_{112} , and C_{166} of germanium (after [26])

exist heavy-doping effects, whereby, for example, the sign of C_{456} reverses at $3 \times 10^{19} \text{ cm}^{-3}$ As doping [42]. The temperature dependence of the third-order constants is represented in Figs. 1.6 and 1.7 [26].

As can be seen from Fig. 1.7, C_{123} and C_{144} exhibit the highest temperature variation, with a positive value at very low temperature. Some local-density-functional approximation calculations of the third-order elastic constants have also been reported [50, 51].

1.2.5 Internal Friction of Ge

One way of obtaining more information on the elastic properties of crystals is by investigating the internal friction (Q_i^{-1}), which can be regarded as the resistance against motion. In practice, internal friction measurements monitor the rate of energy dissipation of crystals undergoing forced periodical vibrations, at small strain levels and in the kilohertz to megahertz frequency range typically (acoustic regime) [52–54]. Such experiments must be performed under good vacuum to avoid energy dissipation by in-diffusing contaminants [53]. If one applies an alternating stress, the vibrational energy ΔW dissipated per cycle relative to W , the total stored vibrational energy at maximal strain, is determined. It has been assumed that this dissipation can happen through two different mechanisms: (1) by viscous motion of dislocations; (2) by stress-induced diffusive motion of point defects [53]. The observation that at the

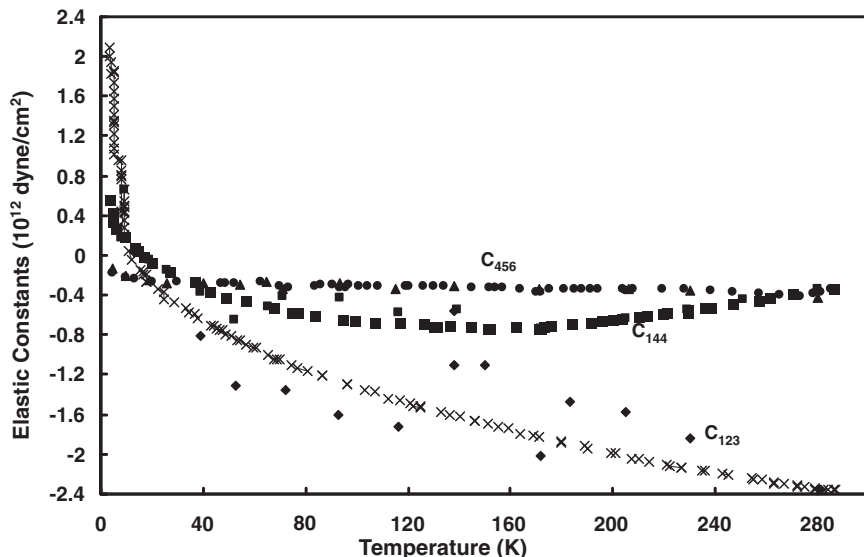


Fig. 1.7. Temperature variation of the third-order elastic constants C_{123} , C_{144} , and C_{456} of germanium (after [26])

dynamic yield point the internal friction showed an abrupt increase has been interpreted in favor of the first mechanism [52].

Early experiments on lowly-doped n-Ge indicated a relaxation peak at 382°C. In deformed crystals, however, no such peak was observed [53]. While it was first suggested that this feature is due to a vacancy drag relaxation in the impurity atmosphere of dislocations, this was soon after questioned by Southgate [55]. He expects from theory that dislocations will affect the internal friction in deformed samples at higher temperatures, with activation energy in the range 1.2 eV. In practice, such a behavior was found above 500°C, showing an activation energy of 1.1 eV [55]. At the same time, the ultrasonic attenuation in germanium in the 20–300 MHz range was ascribed to the damped forced oscillation of dislocation segments [56].

The matter of the origin of the 400°C internal friction peak at $f = 100$ kHz, shown in Fig. 1.8, has been finally settled by Gerck and Williams [57]. It has been ascribed to the acoustic-electric effect and refers to the development of a dc electric field along the direction of propagation of a traveling acoustic wave in a medium containing mobile charges. The response time of the charges to the perturbation is thought to be composed of an intrinsic, temperature-activated lifetime, τ_i , and an extrinsic lifetime, τ_e , of the form of the Shockley-Read-Hall type. An activation energy of 1.1 eV for Ge has been derived [53, 57–59], suggesting that Auger recombination is the origin of the intrinsic recombination at $\sim 400^\circ\text{C}$ [57]. This interpretation was further supported by the fact that as the resonance frequency is changed, the temperature

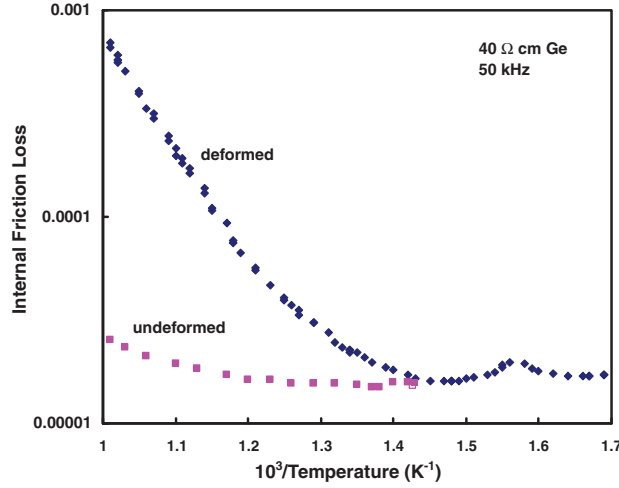


Fig. 1.8. Typical internal friction data of 40 Ω cm germanium at 50 kHz (after [57])

dependence of the peak height is that of the charge carrier density. Moreover, the peak height and location are independent of the type and concentration of impurities, except for very high doping densities and is also independent of the dislocation density N_d [57].

As can be noted in Fig. 1.8, the logarithmic decrement δ (or internal friction loss) increases beyond the 400°C peak, especially for the deformed sample [57]. The loss increases proportionally with N_d and inversely proportional with f , according to the empirical relationship

$$\delta = \frac{N_d \delta_0}{f} \exp(E_i/kT) \left[\frac{n_0}{n_i} \right]^m \quad (1.8)$$

for a strain amplitude in the range 10^{-6} – 10^{-5} . In (1.8) δ_0 is a constant in the range 0.1 – $10 \text{ cm}^2 \text{ s}^{-1}$ for Ge [57] and m is an empirical factor slightly higher than 2 and representing the n-type doping dependence of the dislocation damping. For an electron concentration $n_0 < 10^{17} \text{ cm}^{-3}$ ($< n_i$, the intrinsic carrier concentration at the temperature of the internal friction experiment), the doping factor disappears ($m = 0$), while at high doping concentration, the internal friction loss becomes more pronounced, most likely due to preferential precipitation of the doping impurities on the dislocation cores [57]. On the other hand, it was concluded that impurities like oxygen or copper did not affect the dislocation damping in the high-temperature regime [57]. The intrinsic activation energy E_i is closely connected with the dislocation velocity, as will be discussed further.

It should also be remarked that many investigators found internal friction loss peaks in deformed germanium at much lower temperatures than 400°C, even below room temperature, which were ascribed to the motion of grown-in

single kinks [58–71]. This was related to the fact that from theory a low activation energy for single kink motion E_{SK} (~ 0.1 eV) was anticipated. Later studies revealed much higher values for E_{SK} [72] so that this interpretation has been abandoned. It was suggested that these low temperature loss peaks possibly originate from the motion of hydrogen at the dislocations [67] or from the motion of deformation induced point defects [72].

1.3 Dislocation: Definitions and Structures

The simplest way to view a dislocation is to consider it as the line defect terminating an extra $\{111\}$ half plane of atoms inserted in the otherwise perfect lattice (see Fig. 1.9) and ending on the slip plane 2 [73]. The translational symmetry of the crystal is preserved in the direction of the dislocation but perturbed in radial direction. It is a topological defect, which cannot exist in thermodynamic equilibrium: some thermal or mechanical stress has to be applied to introduce a dislocation. As Ge has an fcc lattice, it has a double $\{111\}$ layer of atoms as in Fig. 1.9. In principle, glide can occur between planes 1 and 2 or between 2 and 3, whereby the spacing has a ratio of 3:1 while the number of bonds to be broken is 1:3, respectively. This means that associated with the two different $\{111\}$ glide planes two main types of dislocations can be considered, belonging to the shuffle set (wide spacing plane 1 and 2) or the glide set (close spacing 2 and 3). While it was originally accepted that glide occurred through the shuffle set, providing a favorable way for easy shear, recent evidence, to be discussed later, casts some doubt on this, so that the matter is unresolved at the moment [74, 75].

Important parameters for a dislocation are the angle α between the dislocation direction and its Burgers or lattice translation vector \mathbf{b} (modulus $b = 0.4$ nm in Ge). For a perfect dislocation, \mathbf{b} is the shortest allowed lattice vector, which for the diamond lattice is $1/2 \langle 110 \rangle$ – half the diagonal of the cubic face or one of the short edges of the tetragonal cell, as can be

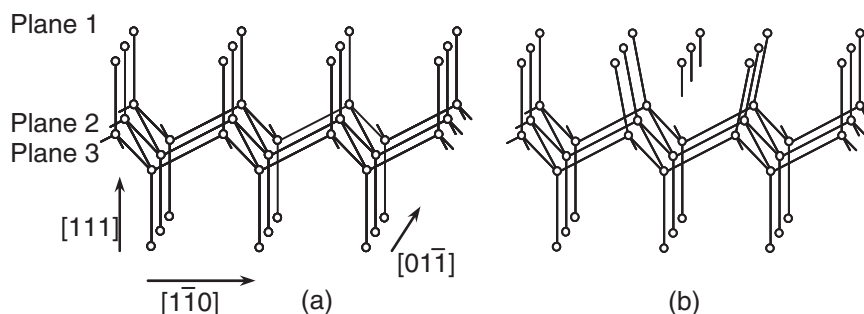


Fig. 1.9. (a) The diamond cubic structure; (b) a 60° dislocation in the diamond cubic structure

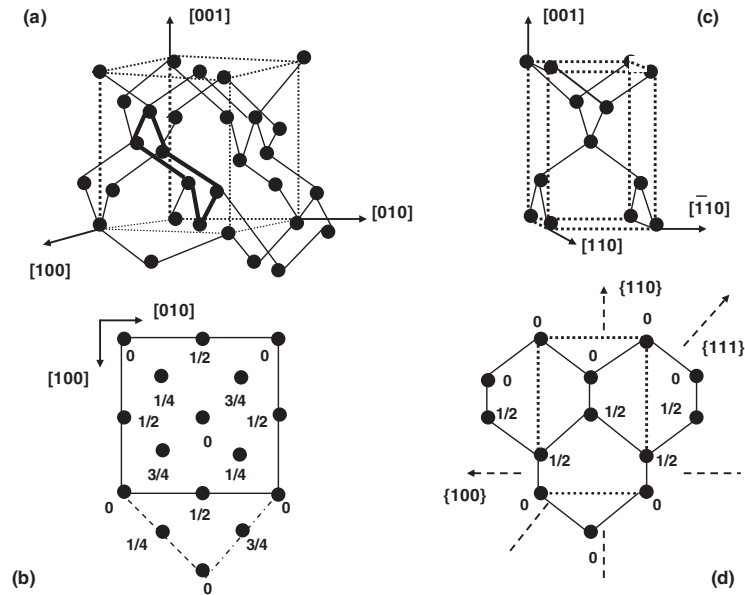


Fig. 1.10. The diamond lattice; the height above the plane of projection is denoted in fractions of the cell dimensions normal to that plane. (a) The cubic unit cell; (b) its projection on (001); (c) the “tetragonal” unit cell; (d) its projection on $\{110\}$. The “tetragonal” unit cell is indicated by broken lines in (b) (after [73])

viewed in Fig. 1.10 [73]. It corresponds to the shortest distance between two equivalent atoms.

In the cubic diamond lattice, both the Burgers vector and the dislocation (axis) lie in $\langle 110 \rangle$ directions. From this follows that there are in principle only three basic types of perfect dislocations to be considered [73], depending on α : a pure edge or 90° dislocation, a 60° dislocation, and a screw (or “ 0° ”) dislocation. The structure of the dominant types in Ge is depicted in Fig. 1.11 [73]. It should be remarked that while the screws have no broken bonds, a row of broken (dangling) bonds exists in the core (along the axis) of a 60° dislocation.¹ As will be seen later, this is believed to be at the origin of the electrical activity of dislocations [6, 67]. Pure edges, introduced by bending (see Sect. 1.4), may also run along a $[11\bar{2}]$ axis with a $1/2 a_0 \langle 110 \rangle$ Burgers vector [70] (a_0 is the lattice parameter).

Real dislocations are only straight along their axis for a few atomic spacings. In practice, defects occur in the dislocation structure, which are called kinks and jogs. A jog is a short piece where the dislocation is interrupted into another orientation [73]. Jogs in an unstable form can act as sources of point defects (vacancies; interstitials) and may impede the mobility of dislocations

¹ Often also called “edge” dislocation, although a pure edge dislocation is characterized by an angle of 90° between its axis and Burgers vector.

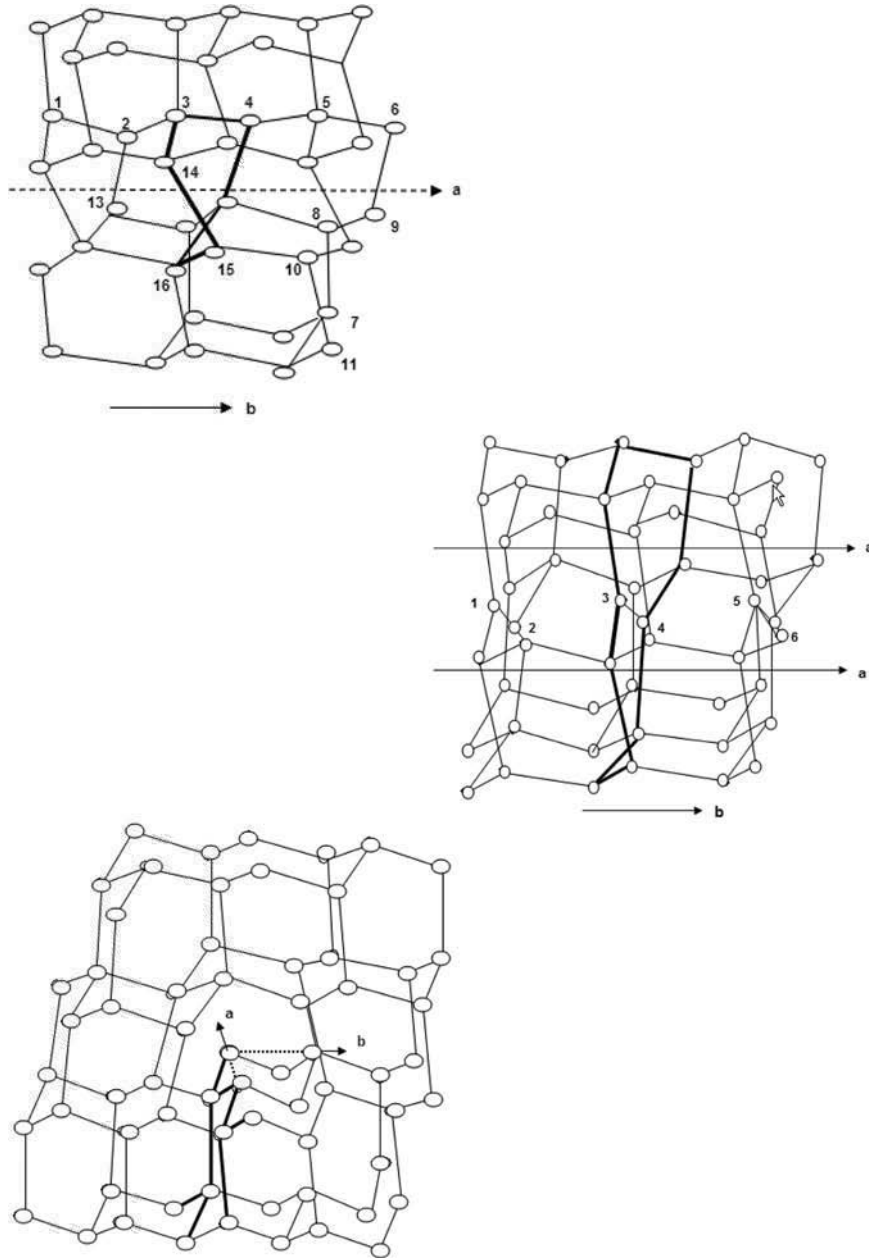


Fig. 1.11. Screw dislocation in the diamond lattice: (*top*) its simplest form; (*middle*) alternative form with double bonds. Corresponding atoms have the same number. *a* Axis, *b* Burgers vector. (*bottom*) 60° dislocation in the diamond lattice; heavy lines denote extra half plane. *a* Axis, *b* Burgers vector (after [73])